Journal of Electrical Engineering, Vol. 74, No. 3, 2023, pp. 197-209

sciendo

PAPER

A powerful PTS strategy boosted by a novel discrete crow search algorithm for reducing the PAPR of UFMC signals

Şakir Şimşir [1*], Necmi Taşpınar[2]

As being one of the main waveform candidates developed for meeting the demands of fifth generation (5G) and beyond telecommunication technologies, universal filtered multicarrier (UFMC) has various appealing features contributing to overcome many obstacles in wireless communication. However, due to the usage of multiple subcarriers, UFMC signals suffer from having high peak-to-average power ratio (PAPR), which has to be kept at low level to prevent the communication quality from being deteriorated. To overcome the problem of high PAPR in the UFMC signals, an advanced version of partial transmit sequence (PTS) was created for PAPR alleviation by integrating an intelligent optimization algorithm in place of its random phase generator. To this end, crow search algorithm (CSA) was utilized. Initially, its novel discrete version called DCSA was developed to make it suitable to be employed in phase sequence optimization, which is a type of combinatorial optimization problem to be solved in discrete space. After the integration of DCSA into the conventional PTS, an advanced PTS variant named DCSA-PTS was created for the UFMC. Optimizing the phase sequences via the DCSA instead of generating them in a random way enhances the performance of PTS scheme. Thanks to the DCSA-based phase optimization, it becomes possible to attain better phase combinations in smaller number of searches. The advantage of using DCSA as a phase optimizer is supported by the simulation results. Due to the superior phase optimization performance of our novel DCSA, the proposed DCSA-PTS strategy clearly outperforms the other schemes considered in this paper.

Keywords: PTS, PAPR, UFMC, 5G, crow search algorithm, discrete crow search algorithm.

1. Introduction

Since the initiation of the first generation (1G) mobile wireless technology consisting of voice-only systems, just a few decades have been enough to reach the fourth generation (4G) cellular technology supporting not only the voice-only communication, but also numerous mobile internet-based services and applications from e-healthcare to mobile gaming entering our lives with smart phones and the other types of smart devices. On the other hand, in the near future, the more advanced applications like smart buildings or cities, unmanned vehicles, intelligent transportation services, virtual reality, etc. will be expected to be supported by the fifth generation (5G) and beyond cellular technologies. It is not hard to predict that the aforementioned applications will be quite common in the next decades with the spread of device to device (D2D) communications, internet of vehicles (IoV) and internet of things (IoT). In order to able to support these manifold incoming applications based on mobile internet, the data rate and quality of service (QoS) need to be upgraded from high to very high levels while the latency have to be taken down to an extremely low level. Besides, high connectivity and reliability are another important two requirements to enable the use of aforementioned applications in incredible diversity [1-4]. Endless technological developments and increasing demands in parallel with this have urged the researchers to develop alternative waveforms to be employed in 5G and beyond cellular technologies since the orthogonal frequency division multiplexing (OFDM) [5, 6] actively used in 4G long term evolution (LTE) physical layer as a basic waveform barely handles these growing demands due to its shortcomings like poor spectral efficiency, the requirement of synchronization and sensitivity to frequency and time offsets. For this reason, a novel waveform named universal filtered multicarrier (UFMC) with unique qualifications was proposed by Vakilian et al. [7]. Some of the advanced features of the UFMC waveform can be put in order as follows: Being possessed of low-level side lobes implying less spectral leakages increases the chance of UFMC to be employed in fragmented spectrum. Thanks to the execution of filtering on equally divided sub-bands, it becomes possible to employ shorter filters and in consequence of this, UFMC becomes appropriate for the short burst transmission. UFMC is also suitable for the transmission via the uplink CoMP manner where CoMP is the abbreviation of "coordinated multi-point" [7-10].

On the other hand, since the UFMC is a multicarrier waveform as the OFDM, the information data is transmitted over multiple subcarriers. However, benefiting from multicarrier transmission strategy gives rise to the formation of high-power peaks in the eventual UFMC transmission signal. For this reason, high peak-to-average power ratio (PAPR), a common problem of multicarrier waveforms, is encountered in the UFMC as well. In order to take the advantage of aforementioned exclusive capabilities of the UFMC waveform having the potential to be a remedy for many problems in wireless communication, the primary obstacle to overcome is the problem of high PAPR in the transmission signals. Because, in practical applications, the transmission signals need

[1] Nevsehir Haci Bektas Veli University, Department of Electrical and Electronics Engineering, Nevsehir, Turkey
[2] Erciyes University, Department of Electrical and Electronics Engineering, Kayseri, Turkey
sakirsimsir@nevsehir.edu.tr

https://doi.org/10.2478/jee-2023-0026, Print (till 2015) ISSN 1335-3632, On-line ISSN 1339-309X

to be amplified prior to be given to wireless channel and it becomes impossible for the related signals to be amplified without any distortion if the PAPRs of them reach to higher levels since widely used types of amplifiers for this task are the nonlinear high-power amplifiers (HPAs) [11, 12], which are designed to have limited power ranges by taking into account the cost-effectiveness and energy efficiency concerns. To put it another way, each time the nonlinear HPA gets out of its amplification range as a result of being pushed by high power components of the transmission signal, serious distortions come into existence in the related signal. Distortive effects of such amplifiers are in proportion to the value of PAPR that the transmission signal has. For this reason, the more the PAPR of a signal is reduced, the less the nonlinear HPA exceeds its amplification range and in consequence of this, the related signal is exposed to less degradation throughout the amplification process.

1.1. Motivation

With the intention of alleviating the signal deteriorations based on the nonlinear HPAs, the researchers developed assorted PAPR minimization methods in the literature. Partial transmit sequence (PTS) strategy [13, 14] comes into prominence with its popularity and widespread usage due to incorporating more than one superior feature. Rather than just being possessed of significant PAPR reduction capability, fulfilling its task in a distortionless way without causing any information loss, having an easy to apply nature facilitating to be employed in diverse multicarrier schemes and possessing very flexible structure enabling both performance improvement and complexity reduction studies via various hybridization or modification implementations make the PTS to be one of the few most used methods in PAPR reduction studies. However, the primitive and outdated random search mechanism makes the conventional PTS a quite complex scheme needing too many random searches to attain a sequence of phase factors ensuring a reasonable PAPR result. In other words, since the improvement in the PAPR value is tried to be provided via ineffective random trials, it becomes impossible to reach even an acceptable PAPR result without carrying out a considerable number of searches in the classical PTS scheme. On the other hand, it is possible to boost the searching capability of the PTS method to obtain better phase sequences in smaller number of searches. The only thing that needs to be done to achieve this goal is to integrate an optimization strategy as a phase optimizer into the PTS scheme. Optimizing the phase sequences based on a specific algorithm will eliminate the most important weakness of the PTS scheme, which is the need for too many searches stemming from its random search mechanism. In order to fulfill the relevant optimization task, we chose an efficient intelligent optimization strategy called crow search algorithm (CSA) [15] in this paper. In spite of its powerful optimization capability, CSA was developed for continuous optimization problems and is not suitable for optimizing the phase sequences consisting of the combinations of discrete numbers like ones and minus ones. For this reason, we first developed its novel discrete version named DCSA and then integrated this new method into the PTS scheme to obtain a robust PAPR reduction strategy called DCSA-PTS in this paper. According to the simulation results, the proposed modern PTS scheme boosted by our novel discrete version of crow search algorithm achieves very promising PAPR improvements in the UFMC signals.

1.2. Related works

It is not likely to come across too many articles handling the high PAPR issue belonging to the UFMC signals in the literature due to the fact that it hasn't been even a decade since the introduction of UFMC to the science community. Almost all the papers dealing with the related issue have been published within the last few years since the researchers have recently begun to focus on this topic. Some of the prominent ones among the aforementioned papers are as follows [16-22]: In [16], the authors proposed a novel companding scheme called modified exponential companding for the UFMC to reduce its PAPR and then improved the PAPR reduction capability of their proposed scheme by combining it with a clipping strategy. In [17], the UFMC signal, which is a multicarrier signal formed by using a certain number of carriers, was transformed to the summation of reduced number of single carrier signals via a precoding scheme. The related reduction in the number of carriers led to significant lowering in the PAPR of UFMC signal while no negative effect arising from the proposed precoding scheme was observed on the bit error rate (BER) performance. In [18], a different SLM approach named decomposed SLM based on the strategy of separating the QAM symbols into real and imaginary parts prior to the phase rotation process was proposed for the mitigation of PAPR escalations in the UFMC signals. In [19], the authors made it feasible to carry out the PTS-based PAPR minimization just before the bandwidth division operation in the UFMC transmitter by attaching an FFT operator to the end of PTS block to render the PAPR-reduced signals appropriate to be split into multiple sub-bands. In this way, it has become possible to get maximal efficiency from the PTS scheme with a simple implementation. In [20], in order to scale down the high PAPR values of the UFMC signals, discrete Hartley transform was utilized as a precoder in the UFMC transmitter. In [21], a different type of SLM strategy through which $U^2/4$ alternative UFMC signals can be produced by exploiting U different phase rotated data sequences was suggested for the UFMC system. In [22], the authors performed PAPR suppression for the UFMC signal through their suggested nonlinear companding transform, in which the signals exceeding a predetermined cut-off point are clipped and the signals having the amplitudes between the cut-off and inflexion points are subjected to nonlinear transform while the remaining ones with low amplitudes are left unchanged.

1.3. Novelties

The novelties contributed by our paper to the science can be listed as follows:

1. A novel discrete model of crow search algorithm (DCSA) has been introduced to the literature.
2. A new type of advanced PTS scheme called DCSA-PTS, in which the DCSA is utilized for the elevation of PTS performance, has been developed.
3. The proposed DCSA-PTS strategy has been integrated to the transmitter of UFMC for the first time to scale down the PAPR of UFMC signal.
4. It is the first time for the crow search algorithm to be exploited in the PTS-based PAPR reduction study.

Paper organization: The paper consists of six sections and the remaining ones of these sections are as follows: In Section 2, the way of utilizing the classical PTS in the transmitter of UFMC to mitigate the PAPR of transmission signal is described. In Section 3, the traditional crow search algorithm in its original form is introduced. After giving an exhaustive explanation of our proposed DCSA-PTS strategy in Section 4, the simulation results are analyzed in Section 5. Last of all, the paper comes to an end with the conclusions part in Section 6.

2. Implementation of PTS-based PAPR Mitigation for the UFMC Signal

The visual description of how to embed the PTS scheme to the UFMC transmitter with the aim of putting the PTS-based PAPR alleviation into practice for the UFMC signals is given in Figure 1 [19]. As it is plain to see from the Figure 1, before proceeding to the operations belonging to the PTS block, the modulation process is executed on the information bits to map them from zeros and ones to QAM symbols, which form the following symbol vector [19]:

$$X(k) = \left[X(0),\ X(1), ..., X(N-1) \right] \tag{1}$$

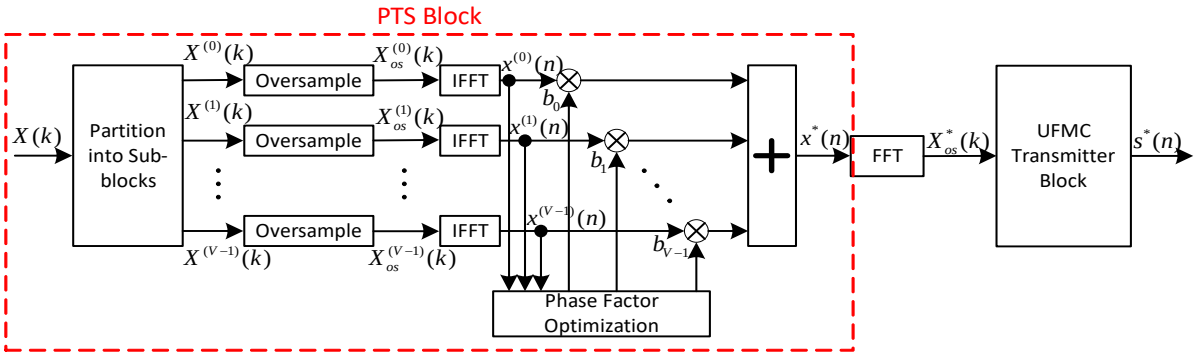

Fig. 1. Application of PTS scheme to the transmitter of UFMC.

Right after the generation of QAM symbol sequence given in Equation (1), the PTS operations are initiated from dividing the vector $X(k)$ into multiple parts called sub-blocks. The key point to be considered when performing the relevant partitioning process is to provide that the sum of the sub-block vectors to be constituted gives the unpartitioned symbol vector $X(k)$ as defined below [19]:

$$X(k) = \sum_{v=0}^{V-1} X^{(v)}(k) \quad , \qquad 0 \le k \le N-1 \tag{2}$$

where V and v correspond to the number of sub-blocks and sub-block index, respectively while $X^{(v)}(k)$ specifies the vth sub-block acquired from the vector $X(k)$. Subsequent to the completion of partitioning process, the lengths of the resultant sub-block vectors are prolonged from N to LN by appending two separate zero sequences in the length $(L-1)N/2$ to their beginnings and ends for the operation of oversampling as indicated below [19]:

$$X_{os}^{(v)}(k) = \left[\underbrace{0,0,...,0}_{(L-1)N/2},\ \underbrace{X^{(v)}(0), X^{(v)}(1), ..., X^{(v)}(N-1)}_{N},\ \underbrace{0,0,...,0}_{(L-1)N/2} \right] \tag{3}$$

In order to make certain of obtaining sufficiently accurate and trustworthy PAPR results, the oversampling factor represented by L needs to be determined as at least 4 ($L \geq 4$) in the simulations [23]. The oversampled frequency domain sub-block vectors expressed in the Equation (3) are then subjected to IFFT operation to get their time domain versions as follows [19]:

$$\begin{aligned} x^{(v)}(n) &= \left[x^{(v)}(0),\ x^{(v)}(1),...,x^{(v)}(LN-1) \right] \\ &= IFFT\left(X_{os}^{(v)}(k) \right),\ 0 \leq v \leq V-1;\ 0 \leq n \leq LN-1 \end{aligned} \tag{4}$$

Together with the last operation, the preparations for the phase rotation process are completed. From now on, the search for the optimal phase sequence can be initiated. To this end, in the first place, the search number symbolized by *SN* parameter is determined. Afterwards, *SN* different phase vectors, each of which has the length of *V*, are generated in a random manner. The related random phase sequences can be defined via the following expression [19]:

$$b_i^{(v)} = \left[b_i^{(0)},\ b_i^{(1)},...,\ b_i^{(V-1)} \right] \quad ,\ \ i = 1,2,...,SN \tag{5}$$

where $b_i^{(v)} \in \{-1,1\}$. Later on, the sub-block vectors are multiplied by these $b_i^{(v)}$ sequences and then recombined subsequent to each multiplication to acquire *SN* different candidate signals from the PTS output in the following way [19]:

$$x_i(n) = \sum_{v=0}^{V-1} b_i^{(v)} x^{(v)}(n) \ , \qquad 0 \leq n \leq LN-1; \quad i = 1,2,...,SN \tag{6}$$

where $x_i(n)$ indicates the *i*th candidate signal attained from the output of PTS by using the *i*th phase sequence $b_i^{(v)}$ in the phase rotation process. Following the *SN* different random trials, the sequence of $b_i^{(v)}$ enabling to achieve the best $x_i(n)$ candidate signal with minimum peak power is appointed as the optimal phase sequence, which is signified by $b_*^{(v)}$. The related appointment among *SN* different phase combinations is carried out by using the operator "arg min $\{\cdot\}$", which finds the optimal $b_i^{(v)}$ minimizing the expression in its parenthesis, as follows [19]:

$$b_*^{(v)} = \arg \min_{b_i^{(v)}} \left\{ \max_{0 \leq n \leq LN-1} \left[\left| \sum_{v=0}^{V-1} b_i^{(v)} x^{(v)}(n) \right|^2 \right] \right\} \tag{7}$$

In the final step, the optimal phase sequence acquired in the Equation (7) is utilized to get the ultimate PTS-based optimized signal from the PTS output as follows [19]:

$$x^*(n) = \sum_{v=0}^{V-1} b_*^{(v)} x^{(v)}(n) \ , \qquad 0 \leq n \leq LN-1 \tag{8}$$

Subsequent to making the signal $x^*(n)$ feasible for the UFMC input by acquiring its frequency domain equivalent via the FFT process, the UFMC transmitter operations are applied to the resultant $X_{os}^*(k)$ signal, which corresponds to the oversampled version of the phase rotated optimum data sequence in the frequency domain, one by one and finally, the eventual signal $s^*(n)$ acquired from the UFMC output will be possessed of minimized PAPR. One can find detailed mathematical descriptions of the aforementioned operations from [19].

3. Crow search algorithm

The smart behaviors of the crows inspired Askarzadeh in developing a new optimization technique called crow search algorithm (CSA) in 2016 [15]. In the CSA, each crow is defined as a *d*-dimensional solution vector specifying the position of *i*th crow at the iteration *t* in the search environment as follows:

$$x_i^t = \left[x_i^t(1),\ x_i^t(2),...,\ x_i^t(d) \right],\ i = 1,2,...,P;\ \ t = 1,2,...,t_{\max} \tag{9}$$

where P and $t_{\max}$ represent the size of crow population and maximum number of iterations, respectively. Apart from this, in order to keep the best food positions achieved so far, a memory vector is defined for each crow in the following way:

$$m_i^t = \left[m_i^t(1),\ m_i^t(2),...,\ m_i^t(d) \right],\ i = 1,2,...,P;\ \ t = 1,2,...,t_{\max} \tag{10}$$

The related food position represented by the vector m_i^t is kept in the memory by the *i*th crow until the discovery of better one. The position update for each crow is carried out in the following manner: First of all, for each iteration, it is assumed that the crow *j* controls its hidden food by visiting its hiding position denoted by the vector m_j^t. When the crow *i* follows the *j*th crow to get an idea regarding the place of its hidden food, two different cases may arise [15]:

***Case 1*:** If the *j*th crow doesn't become aware of being followed by the *i*th crow, the crow *i* will find an opportunity to approach to the position of hidden food belonging to the crow *j*. In this case, the position update of the crow *i* will be carried out as follows:

$$x_i^{t+1} = x_i^t + r_i \times fl \times \left(m_j^t - x_i^t \right) \tag{11}$$

where r_i denotes the uniformly distributed random number in the range (0,1) and *fl* corresponds to the flight length.

***Case 2*:** If the crow *j* becomes aware of being followed by the crow *i*, it flies to a random place for the purpose of preventing the place of its hidden food from being detected by the crow *i*. In this case, the new position of the crow *i* will be a random place in the search space as well.

It is possible to express both cases by using the awareness probability (*AP*) indicating the probability of crow *j* to become aware of being followed. Hereby, the position and memory updates for the crow *i* can be expressed in the following manner, respectively:

$$x_i^{t+1} = \begin{cases} x_i^t + r_i \times fl \times \left(m_j^t - x_i^t \right), & if\ \ r_j \geq AP \\ a\ random\ position, & if\ \ r_j < AP \end{cases} \tag{12}$$

$$m_i^{t+1} = \begin{cases} x_i^{t+1}, & if\ \ f\left(x_i^{t+1} \right)\ is\ better\ than\ f\left(m_i^t \right) \\ m_i^t, & otherwise \end{cases} \tag{13}$$

where r_j signifies a random number uniformly distributed in the range (0,1) and $f(\cdot)$ represents the objective function utilized for calculating the fitness values of the crow positions. The position and memory updates of each crow are carried out via Equations (12) and (13), respectively for each iteration. After repeating the aforementioned update operations throughout $t_{\max}$ iterations, the best position existing in the crow memories is determined as the optimal solution achieved by the algorithm.

4. The proposed PTS strategy empowered by our novel discrete crow search algorithm

The CSA is a robust optimization procedure utilized in many kinds of engineering problems in different fields. However, it is not feasible to directly apply its primary version, which is designed for optimizing the parameters that can take continuous values within a predefined range, to our phase optimization problem since each dimension of the $b_i^{(v)} = \left[b_i^{(0)},\ b_i^{(1)},...,\ b_i^{(V-1)} \right]$, $i = 1,2,...,SN$ representing the sequence of phase factors to be optimized can be equal to either one or minus one. In other words, due to the fact that the original CSA is not developed for the discrete optimization problems, it is not possible to optimize the phase vectors consisting of different −1 and +1 combinations by using its initial form compatible with the continuous optimization problems. In order to get over this issue that prevents the CSA from being utilized in our problem, an effective discrete CSA variant called DCSA has been developed in this paper. Later on, the relevant new discrete model of CSA has been integrated to the PTS scheme as a phase optimizer to upgrade its PAPR reduction capability. In the resultant joint PAPR reduction strategy called DCSA-PTS, the phase vectors to be optimized are expressed as the crow positions as follows:

$$b_s^{(v)} = \left[b_s^{(0)},\ b_s^{(1)},...,\ b_s^{(V-1)} \right], \quad s = 1,2,...,S \tag{14}$$

where *S* corresponds to the swarm size of the crows and *s* is the crow index indicating the crow to which the relevant position vector belongs. Step by step implementation of the phase optimization process using DCSA in the PTS scheme is yielded below:

Step 1: The crow flock is initialized by generating *S* random crow positions expressed by the Equation (14). Later on, the initial crow memories are determined as the first crow positions. The memory vector belonging to the crow *s* is defined in the following manner:

$$m_s^{(v)} = \left[m_s^{(0)},\ m_s^{(1)},...,\ m_s^{(V-1)} \right] \quad , \quad s = 1, 2, ..., S \tag{15}$$

Step 2: The initial crow positions are evaluated by calculating their fitness values through the following fitness function:

$$fit\left(b_s^{(v)}\right) = \max_{0 \le n \le LN-1} \left[\left| \sum_{v=0}^{V-1} b_s^{(v)} x^{(v)}(n) \right|^2 \right] , \ s = 1, 2, ..., S \tag{16}$$

Step 3: For each crow in the flock, one random number symbolized by $r_s \in [0,1]$ is generated. After that, the related random number generated for the crow *s* is compared to the parameter *AP* determined before the optimization process in the range [0, 1].

Step 4: If $r_s \ge AP$, one neighbor solution is produced for the crow *s* via the cyclic bit flipping procedure [24] put into practice by using a flipping operator specialized to fulfill this operation as follows:

$$b_s^{(v),new} = flip\left(b_s^{(v)}\right)_{\phi_s} \tag{17}$$

In the above equation where $b_s^{(v)} \in \{-1,1\}$, the operator $flip\left(b_s^{(v)}\right)_{\phi_s}$ reverses the sign of the element existing in the ϕ_s th dimension of the vector $b_s^{(v)}$, which consists of *V* dimensions in total as already known. By the way, it is important to note that the parameter ϕ_s symbolizing the flipping index of the *s*th crow in the flock is appointed as $\phi_s = 1$ for each crow at the beginning. Following the fulfillment of flipping operation, the greedy selection between the new and old positions represented by $b_s^{(v),new}$ and $b_s^{(v)}$, respectively is carried out with respect to their fitness values. Namely, if the fitness of $b_s^{(v),new}$ is better than that of $b_s^{(v)}$, the vector $b_s^{(v),new}$ is accepted as the new position of the crow *s*. Otherwise, the vector $b_s^{(v)}$ is retained as the current solution of the related crow. Apart from this, if $b_s^{(v),new}$ has better fitness quality than that of the memory vector $m_s^{(v)}$ keeping the current best position of the crow *s*, the memory of the relevant crow is updated by replacing $m_s^{(v)}$ with the $b_s^{(v),new}$. Otherwise, $m_s^{(v)}$ is maintained to be kept as the current best solution of the crow *s* without any change. Subsequent to the aforementioned position and memory updates, the parameter ϕ_s is increased by one to make sure that the next implementation of bit flipping, which is repeated for the crow *s* each time the condition $r_s \ge AP$ is provided in the upcoming iterations, proceeds from the component next to the recent flipped one in the vector $b_s^{(v)}$:

$$\phi_s = \phi_s + 1 \tag{18}$$

Right after the increment of ϕ_s by one, the following operation needs to be applied to guarantee that the process of bit flipping is maintained in a cyclical manner for each crow position:

$$\phi_s = \mathrm{mod}\left(\phi_s - 1,\ V\right) + 1 \tag{19}$$

The modulo operator existing in the equation above is used to get the remainder from the division of $(\phi_s - 1)$ by *V*. The basic function of the Equation (19) is to return the value of ϕ_s to 1 every time it exceeds *V*. The control of ϕ_s value via the Equation (19) following its each increment makes it possible to keep the bit flipping process moving in cyclic mode throughout the progress of iterations. Owing to the utilization of aforementioned cyclic bit flipping procedure, the crows are not allowed to leave unvisited positions around their neighborhoods for a long time throughout the optimization process.

Step 5: If $r_s < AP$, the crow *s* is moved to a random position in the search space by mutating some of the bits in its position vector, randomly via the following mutation operator:

$$b_s^{(v)} = \underset{0 \le v \le V-1}{\mathrm{mut}} \left(b_s^{(v)}, NB\right) \tag{20}$$

The mutation operator given in the above equation reverses the signs of *NB* bits in different dimensions determined randomly in the range $0 \le v \le V-1$ where the *NB* parameter specifies the number of bits to be mutated.

Step 6: The operations from Step 3 to Step 5 are repeated for each crow existing in the *S*-sized flock. By keeping in mind that *S* times repetition of the operations in the relevant range corresponds to the one iteration of DCSA-PTS procedure, the optimization

process is carried on for t_{max} iterations. Subsequent to the termination of the optimization process, the best memory vector with the highest fitness quality is appointed as the optimal phase sequence.

The main idea in developing the DCSA is to provide an efficient phase optimizer for the conventional PTS scheme by sticking to the main structure of the original CSA. When developing our proposed discrete version, not only the main structure of the original CSA was kept, but also an efficient procedure called cyclic bit flipping was integrated to the related algorithm. Thanks to this modification, each crow has gained the ability to make a systematic search in discrete space without leaving unvisited positions around their neighborhoods. In addition to this, a mutation operator was defined to prevent the algorithm from getting stuck in local minimums by taking the advantage of mutation operation in a controlled way.

5. Simulation results

In this section, in order to get strong evidences about the performance level of our suggested scheme among the modern PTS techniques upgraded by the meta-heuristic algorithms, two advanced PAPR reduction schemes with the name of TS-PTS and DFA-PTS, are taken into consideration for the benchmarking purpose. In the aforementioned benchmark schemes, while the first one was created with the integration of very famous and successful optimization algorithm called tabu search (TS) [24], the latter is based on the discrete firefly algorithm [25], one of the most efficient and frequently utilized meta-heuristic approaches developed in recent years. The parameter appointments carried out for the simulations are demonstrated in Table 1.

Table 1. Simulation parameters

Parameter	Symbol	Value
Number of UFMC sub-bands	B	8
Model of sub-band filter	−	Dolph-Chebyshev
Length of filter	L_f	64
Type of modulation	−	16-QAM
Number of subcarriers	N	128
Size of FFT	−	1024
Cyclic prefix length	L_{CP}	64
Oversampling factor	L	8
Channel type	−	AWGN
Sampling frequency	−	15.36 MHz
Model of HPA	−	SSPA
Number of searches	SN	256
Number of PTS sub-blocks	V	64

Table 2. Investigation of the considered schemes with regard to their search complexities

Techniques	Search Numbers (SN)	PAPR
DCSA-PTS	$S \cdot t_{max} = 2 \cdot 128 = 256$	6.49 dB
DFA-PTS	$FlyNum \cdot G_{max} = 4 \cdot 64 = 256$	6.72 dB
TS-PTS	$(V - L_T) \cdot C_{max} = (64 - 48) \cdot 16 = 256$	6.85 dB
PTS	256	6.99 dB
Original	0	11.35 dB

In Table 2, the expressions of the search complexities corresponding to the number of searches were acquired in the middle column for each PTS-based strategy. With a view to carry out an equitable performance comparison, the value of each complexity expression is fixed to 256 in this paper as demonstrated in the same column. On the other hand, the right column of the Table 2 contains the PAPR achievements of the considered schemes at CCDF = 10^{-3} in the case that their search complexities are equalized to the value of 256. As can be seen from the bottom row of the Table 2, in case of not performing any PAPR reduction in the original signal, the search cost naturally becomes equal to zero. If we get to the next row from the bottom one, it will be seen that the search cost ascends from $SN = 0$ to $SN = 256$ with the application of conventional PTS to the original signal for PAPR mitigation. In the classical PTS procedure, the search complexity, namely the number of searches, is determined by the number of PAPR computations to be executed throughout the PAPR reduction process. Since SN different randomly generated phase sequences cost

SN number of PAPR calculations, it becomes possible to set the search complexity to a certain value by determining the total number of phase sequences in the PTS scheme. For this reason, in order to make the search complexity of PTS equal to $SN = 256$, which is the common value appointed for each scheme in our paper, the number of phase sequences to be generated is determined as 256 prior to the PAPR reduction process. When dealing with the definition of search complexities in the state-of-art PTS schemes reinforced by the meta-heuristic algorithms, the key point to focus on is the number of fitness calculations performed from the initiation to the termination of the optimization process. With that knowledge in mind, the search complexity expression of our proposed DCSA-PTS technique will be obtained as $SN = S \cdot t_{\max}$ due to the fact that the multiplication of swarm size (S) by the maximum number of iterations ($t_{\max}$) directly gives the aggregate number of fitness calculations denoting the number of searches in such types of PTS procedures based on meta-heuristic approaches. As a consequence of an exhaustive experimental study, which has been repeated for each of the considered meta-heuristic-based PTS schemes to achieve the optimal parameter combination enabling maximal performance, the parameters of DCSA were determined as $S = 2$, $t_{\max} = 128$, AP=0.01 and NB=3 where AP and NB represent the awareness probability and the number of bits to be mutated, respectively. When considering the second advanced PTS procedure called DFA-PTS, similar to the DCSA-PTS strategy, the multiplication of two parameters named the number of fireflies (*FlyNum*) and maximum generation number (G_{max}) gives the definition of search complexity as $SN = FlyNum \cdot G_{max}$ where the parameters of *FlyNum* and G_{max} were appointed as $FlyNum = 4$ and $G_{max} = 64$. Apart from the aforementioned two parameters, the remaining DFA parameters symbolized by α and γ were specified as $\alpha = 2$ and $\gamma = 0.003$ where α corresponds to the random step size and γ represents the coefficient of light absorption. At last, the search complexity of the last modified PTS scheme given the name of TS-PTS is defined as $SN = (V - L_T) \cdot C_{max}$ where the difference between the parameters V and L_T corresponding to the length of solution vector and length of tabu list, respectively is multiplied by the maximum number of cycles (C_{max}) to acquire the total number of fitness computations. Except for the parameter V, which has to be equal to the number of sub-blocks specified as 64 in our paper, the parameters peculiar to the TS algorithm were assigned as $C_{max} = 16$ and $L_T = 48$. Table 2 puts forth a serious evidence regarding the superior performance of the DCSA-PTS procedure in PAPR suppression. As it is quite obvious in Table 2, when equalizing the search complexities of the considered schemes to $SN = 256$, the proposed DCSA-PTS strategy manages to reach the lowest PAPR level at CCDF = 10^{-3}.

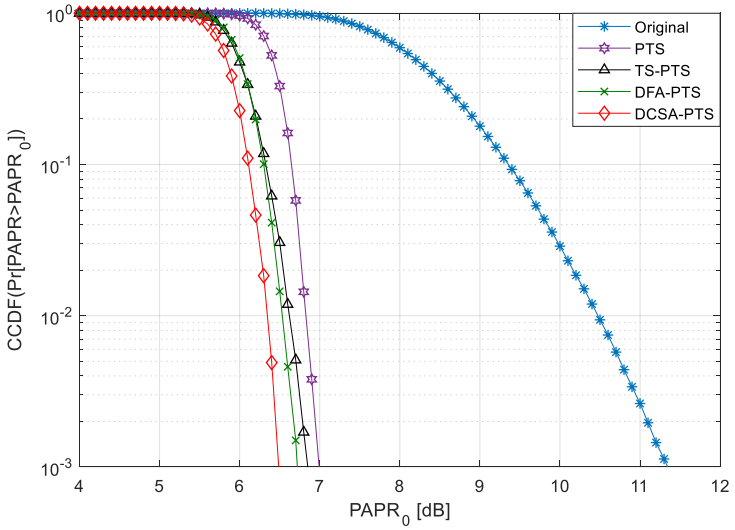

Fig. 2. Comparative analysis of the considered schemes via their $PAPR_0$ [dB] – CCDF curves.

In Figure 2, the most common performance evaluation procedure utilized in almost all PAPR reduction studies was put into practice for the considered strategies by obtaining the $PAPR_0$ [dB] – CCDF curve of each one. One can clearly see from the Figure 2 that no matter which optimization technique is employed, the phase optimization process has a great effect on bringing down the PAPR level that can be achieved by the conventional PTS to the lower levels. The main issue here is to what extent you can reduce the relevant PAPR level. Our proposed DCSA does a great job in this regard. It provides 0.50 dB PAPR gain over the classical PTS method at CCDF = 10^{-3} by making 0.23 dB and 0.36 dB differences to the DFA and TS algorithms, respectively. Making more than 0.20 dB difference even to its closest competitor clearly reveals how effective the DCSA is in optimizing the phase sequences of PTS scheme.

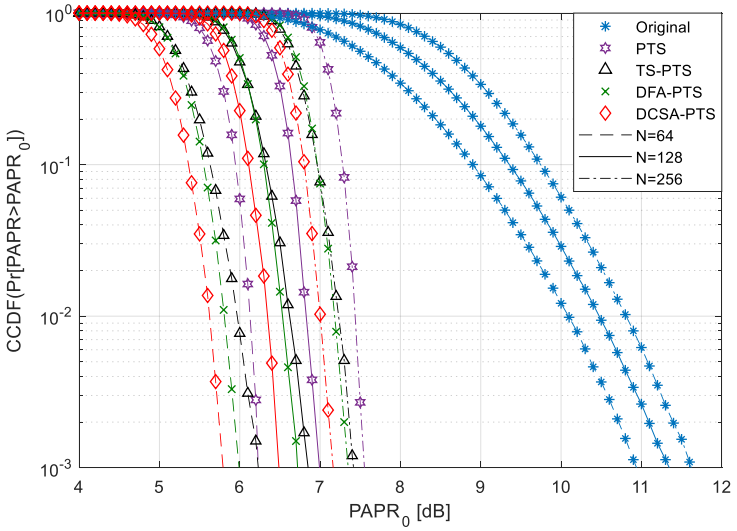

Fig. 3. The subcarrier impact on the performance of DCSA-PTS and the other benchmark strategies.

In Figure 3, the number of subcarriers, which is determined as 128 in our paper is both doubled and cut in half for the purpose of putting the proposed DCSA-PTS strategy to the test regarding its performance steadiness in different subcarrier conditions. The blocks of $PAPR_0$ [dB] – CCDF curves obtained for three different number of subcarriers evidently demonstrates that the aforementioned changes in the number of subcarriers cannot keep the DCSA-PTS from preserving its predominant performance over the other techniques. It maintains its performance superiority for both the twice and half of the 128 subcarriers. For instance, if we concentrate on the PAPR values achieved by the DCSA-PTS and DFA-PTS, which is the nearest method to our proposed scheme in terms of PAPR reduction performance, the PAPR differences between these two techniques at CCDF = 10^{-3} for 64, 128 and 256 subcarriers are grasped from the Figure 3 as 0.20 dB, 0.23 dB and 0.19 dB, respectively. As it can be comprehended from the above outcomes, DCSA-PTS scheme manages to keep the difference with its closest rival at minimum 0.19 dB.

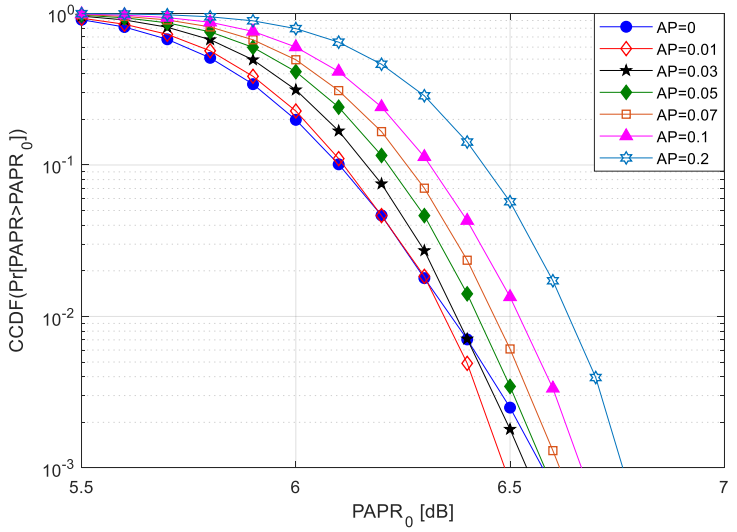

Fig. 4. The influence of awareness probability on PAPR achievement of the DCSA-PTS strategy.

In Figure 4, seven different values varied from 0 to 0.2 are given to the parameter of awareness probability symbolized by *AP* to test its effect on the DCSA-PTS performance. While varying the value of *AP* in the range [0, 0.2], the other DCSA parameter signified by *NB* is kept constant at its predefined value, which is equal to 3. As can be distinguished from the Figure 4, setting the parameter *AP* to a value in the range [0, 0.03] results in relatively better PAPR reduction performance. The remaining *AP* values beyond this range causes significant performance deteriorations in the DCSA-PTS strategy. In the related range, while the increase of *AP* from 0 to 0.01 ensures the DCSA-PTS to achieve its best PAPR reduction performance, maintaining to raise the awareness probability from 0.01 to 0.03 leads to a notable performance worsening. After exceeding the range [0, 0.03], each increase in the value of *AP* does nothing but make the performance of DCSA-PTS even worse. For instance, while the adjustment of *AP* to the values of 0, 0.01 and 0.03 provides the DCSA-PTS to acquire 6.58 dB, 6.49 dB and 6.54 dB PAPR values at CCDF = 10^{-3}, carrying

on to increase the value of *AP* from 0.03 to 0.2 causes the PAPR of DCSA-PTS to increase up to 6.76 dB at the relevant CCDF value. The reason for why too much increase in the parameter *AP* leads to the performance degradation in the DCSA-PTS strategy can be explained as follows: As it is known from the Section 5, the higher *AP* increases the chance of every crow in the population to be mutated via the Equation (20) at each iteration. Since the higher frequency of mutation leads to the deteriorations in the solutions achieved so far, too much increase in the value of *AP* controlling the mutation probability causes the performance of DCSA-PTS to decrease as clearly seen from the Figure 4.

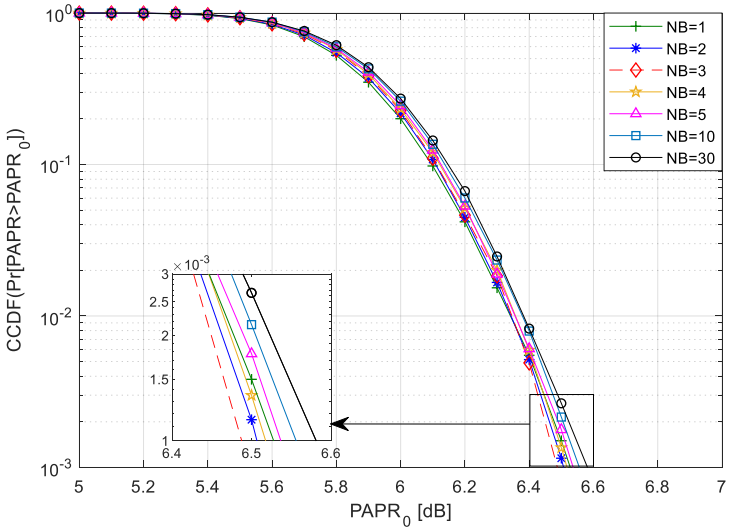

Fig. 5. The investigation of DCSA-PTS performance for diversified NB values.

In Figure 5, the performance of DCSA-PTS is examined for distinct values of *NB* parameter specifying the number of bits to be mutated in DCSA. For that purpose, a series of $PAPR_0$ [dB] – CCDF curves were plotted for the DCSA-PTS scheme by assigning diversified values to the parameter *NB*. In order to carry out more comprehensive parameter analysis and not to leave any question mark in minds, the value of *NB* is altered in a sufficiently broad range from 1 to 30. During the variation of *NB* in the range [1, 30], the parameter *AP* is kept fixed at 0.01 value. When looking at the Figure 5, the first thing that catches the eye is the proximity of the $PAPR_0$ [dB] – CCDF curves to each other. When focusing on the PAPR values of the related curves at CCDF = 10^{-3}, it will be seen that the difference between the highest and lowest PAPR values acquired by adjusting the value of *NB* to 30 and 3, respectively is equal to only 0.09 dB. If we take a closer look at the existing curves, we will get a chance to see the effect of each *NB* variation on the DCSA-PTS performance. For instance, the increase of *NB* from 1 to 3 leads to a steady decrement in the PAPR from 6.53 dB to 6.49 dB at CCDF = 10^{-3}. However, starting from the value of 4, maintaining to increase the parameter *NB* towards the value of 30 causes the PAPR to rise again. For example, when the lowest PAPR level, which is equal to 6.49 dB, is achieved by setting the *NB* to 3, one increase in the value of *NB* will give rise to 0.03 dB regrowth in the related PAPR value and if the increase of *NB* is maintained up to the value of 30, the PAPR of DCSA-PTS will reach to the level of 6.58 dB at CCDF = 10^{-3}. As can be deduced from these results, it is important to adjust the value of *NB* to an optimal value to balance the local exploitation and global exploration capability of the DCSA. Since the parameter *NB* determines the number of bits to be mutated in the solution vector, too much increase in the value of *NB* causes deteriorations in each solution and accordingly performance decline in the DCSA-PTS strategy. Likewise, giving very small values to the parameter *NB* leads to the performance worsening as well due to the fact that too much decrement in the value of *NB* reduces the global exploration capability of DCSA.

In Figure 6, in order to see to what extent the considered strategies can reflect their PAPR achievements to the side lobe suppression performance, PSD curves of PAPR reduced UFMC signals are obtained for each strategy in one graph. In addition to this, the influence of input back off (IBO) parameter, the value of which determines the distance of amplification point to the saturation region in the SSPA, on the side lobe levels of the PAPR reduced signals is tested in the same graph by obtaining the aforementioned PSD curves for three different IBO values. Aside from the IBO, there exists one more SSPA parameter named smoothness (*p*). During the variation of IBO from 10 dB to 12 dB, the parameter *p* controlling the sharpness of the transition from linear region to the saturation region in the SSPA is kept at the value of 3. PAPR lowering has a great benefit on mitigating the SSPA-based signal deteriorations. For this reason, it is crucial to use a powerful PAPR reduction strategy to minimize the aforementioned nonlinear distortions and associated performance worsening such as the side lobe risings and BER increments. To put it another way, the amount of side lobe suppression depends on how efficient scheme is utilized for PAPR reduction. From this perspective, since the DCSA-PTS scheme is the one capable of acquiring the lowest PAPR value among the considered schemes, it is also expected from the related scheme to achieve the lowest side lobe level as well by ensuring maximum side lobe suppression. Figure 6 confirms this expectation. For instance, while the level of side lobes belonging to the conventional PTS procedure

at IBO = 11 dB is suppressed from −45.75 dB to −50.20 dB and −51.12 dB by the TS-PTS and DFA-PTS methods respectively, it becomes possible to obtain 3.19 dB more suppression via the suggested DCSA-PTS procedure in comparison to the DFA-PTS scheme. Thus, by reaching the level of −54.31 dB, the amount of 8.56 dB suppression is achieved at the related IBO value via our proposed scheme in the side lobe level of classical PTS technique in total. On the other hand, the deterioration degree of a signal not only depends on its PAPR level, but also how far it is amplified from the saturation region of the SSPA. Even though the PAPR of a signal is reduced to the lowest levels, adjusting the amplification point too close to the saturation region by assigning smaller values to the IBO parameter will increase the frequency of reaching the saturation in the SSPA and accordingly the amount of distortion in the signal to be amplified. For this reason, the higher IBO values bring about less signal distortions and accordingly the lower side lobe levels as verified by Fig. 6.

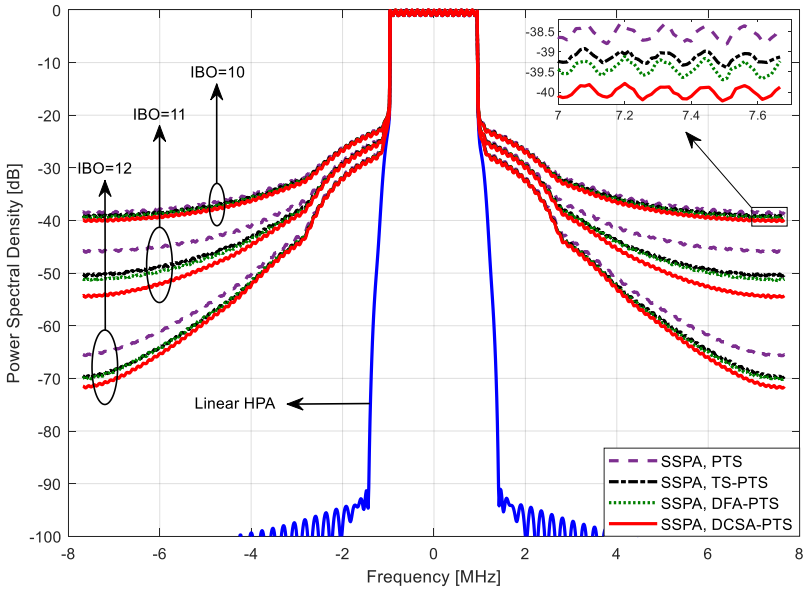

Fig. 6. Comparison of PSD curves obtained with the usage of considered methods for varied IBO values.

Another positive consequence of the PAPR reduction process is the BER improvement. The last simulation study was carried out to confirm the related benefit of the PAPR lowering strategies. For that purpose, three different BER curves were plotted for each scheme in Figure 7 to put their BER performances to the test at 7 dB, 8 dB and 9 dB IBO values while the parameter of smoothness in SSPA was set to 1. Whatever effect the PAPR minimization and IBO increment have on the PSD performance, they have the same effect on the BER performance as well. To put it more clearly, both the increase in the success of PAPR minimization and ascension in the value of IBO will directly result in better BER performance. For instance, as the most successful PAPR reduction procedure, DCSA-PTS achieves the lowest BER at each IBO value. If it is concentrated on the BER values achieved for IBO = 8 dB at 30 dB signal-to-noise ratio (SNR) value, it will be seen that the BERs of the DCSA-PTS and the other benchmark strategies from the lowest to the highest value are equal to 4.05×10^{-4}, 5.12×10^{-4}, 5.74×10^{-4} and 8.29×10^{-4}, respectively. Apart from this, every IBO increase results in a certain amount of BER improvement in each method. It is possible to see the related IBO effect from the BER results of our proposed scheme. If it is focused on the BER achievement of the DCSA-PTS scheme at SNR = 22 dB, the BER values achieved by our proposed scheme for the varied IBO values from 7 dB to 9 dB will be read from the Figure 7 as 6.72×10^{-3}, 1.41×10^{-3} and 2.14×10^{-4}, respectively.

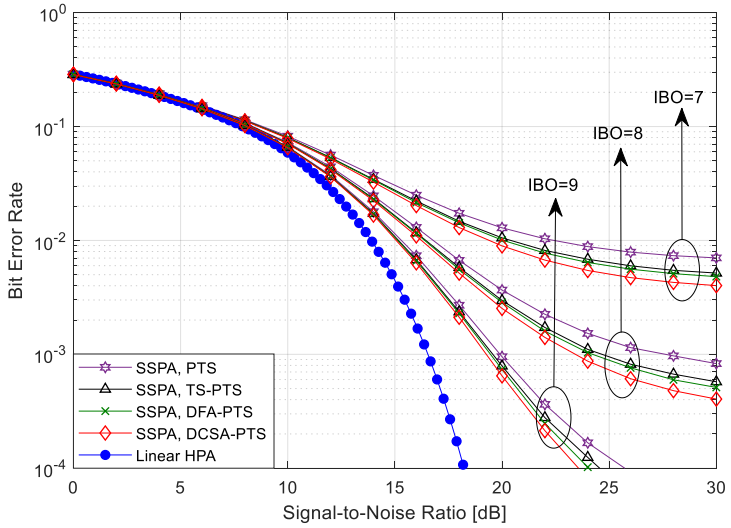

Fig. 7. SNR [dB] – BER curves of the considered schemes for several IBOs.

6. Conclusion

In this study, an efficient discrete variant of the crow search algorithm, given the name of DCSA in this paper, was developed to create an empowered form of the partial transmit sequence scheme called DCSA-PTS, in which the role of our newly designed DCSA is to enable the conventional PTS scheme to reach better results with less number of searches by optimizing the phase factors. Following the aforementioned upgrade in the classical PTS method, the resultant DCSA-PTS strategy was put into practice in the transmitter of UFMC with the intention of lowering the high-level PAPR values of the UFMC signals. A comprehensive simulation study was carried out to assess the performance of our proposed scheme. As well as the utilization of $PAPR_0$ [dB] – CCDF graphs to observe how much PAPR gain is ensured by the DCSA over the classical PTS scheme, PSD and SNR [dB] – BER analyzes were also added to the simulation study to evaluate the DCSA-PTS performance from three different angles. Moreover, in order to be fully sure whether the DCSA provides a satisfying improvement in the PTS performance and acquire more convincing results demonstrating the efficiency of our proposed DCSA-PTS strategy, two robust PTS schemes strengthened by TS and DFA algorithms, the effectiveness of which have been proven many times by manifold studies in the literature, were incorporated into the simulation study for comparison. According to the simulation results, DCSA-PTS has become by far the best performing PAPR reduction strategy by achieving significantly more performance gain over the PTS scheme compared to the TS-PTS and DFA-PTS methods.

Acknowledgment

This work was supported by the Scientific Research Projects Coordinating Unit of Erciyes University [Grant Number: FDK-2018-8463].

References

[1] M. Agiwal, A. Roy, and N. Saxena, “Next generation 5G wireless networks: a comprehensive survey,” IEEE Communications Surveys & Tutorials, vol. 18, no. 3, pp. 1617-1655, 2016.

[2] S.-Y. Lien, S.-L. Shieh, Y. Huang, B. Su, Y.-L. Hsu, and H.-Y. Wei, “5G new radio: waveform, frame structure, multiple access, and initial access,” IEEE Communications Magazine, vol. 55, no. 6, pp. 64-71, 2017.

[3] A. R. Asif, F. Zahra, and M. A. Matin, “Cognitive solution for IoT communication technologies – emphasis on 5G,” Journal of Electrical Engineering, vol. 71, no. 2, pp. 131-137, 2020.

[4] I.F. Akyildiz, S. Nie, S.-C. Lin, and M. Chandrasekaran, “5G roadmap: 10 key enabling technologies,” Computer Networks, vol. 106, pp. 17−48, 2016.

[5] L.J. Cimini, “Analysis and simulation of a digital mobile channel using orthogonal frequency division multiplexing,” IEEE Transactions on Communications, vol. 33, no. 7, pp. 665−675, 1985.

[6] S. Tabassum, S. Hussain, and A. Ghafoor, "Peak to average power ratio reduction in NC-OFDM systems," Journal of Electrical Engineering, vol. 66, no. 3, pp. 154-158, 2015.
[7] V. Vakilian, T. Wild, F. Schaich, S. T. Brink, and J. F. Frigon, "Universal-filtered multi-carrier technique for wireless systems beyond LTE," IEEE Globecom Workshops (GCWkshps), Atlanta, GA, USA, pp. 9-13, 2013.
[8] J. Wen, J. Hua, W. Lu, Y. Zhang, and D. Wang, "Design of waveform shaping filter in the UFMC system," IEEE Access, vol. 6, pp. 32300–32309, 2018.
[9] Y. Li, B. Tian, K. Yi, and Q. Yu, "A novel hybrid CFO estimation scheme for UFMC-based systems," IEEE Communications Letters, vol. 21, no. 6, pp. 1337–1340, 2017.
[10] M. Wu, J. Dang, Z. Zhang, and L. Wu, "An advanced receiver for universal filtered multicarrier," IEEE Transactions on Vehicular Technology, vol. 67, no. 8, pp. 7779–7783, 2018.
[11] M. C. P. Paredes, F. Grijalva, J. C. Rodrigez, and F. Sarzosa, "Performance analysis of the effects caused by HPA models on an OFDM signal with high PAPR," IEEE Second Ecuador Technical Chapters Meeting (ETCM), Salinas, Ecuador, pp. 1-5, 2017.
[12] H. G. Ryu, J. S. Park, and J. S. Park, "Threshold IBO of HPA in the predistorted OFDM communication system," IEEE Transactions on Broadcasting, vol. 50, no. 4, pp. 425–428, 2004.
[13] L. J. Cimini, and N. R. Sollenberger, "Peak-to-average power ratio reduction of an OFDM signal using partial transmit sequences," IEEE Communications Letters, vol. 4, no. 3, pp. 86-88, 2000.
[14] Ş. Şimşir, and N. Taşpınar, "Cumulative symbol optimization–based partial transmit sequence technique for PAPR reduction in low complexity GFDM system," Transactions on Emerging Telecommunications Technologies, vol. 31, no. 6, pp. 1–19, 2020.
[15] A. Askarzadeh, "A novel metaheuristic method for solving constrained engineering optimization problems: Crow search algorithm," Computers & Structures, vol. 169, pp. 1-12, 2016.
[16] V.D. Chintala, and A. Sundru, "An optimal nonlinear companding transform with clipping scheme for universal filtered multicarrier systems," International Journal of Communication Systems, vol. 33, no. 16, pp. 1–21, 2020.
[17] M.B. Mabrouk, M. Chafii, Y. Louet, and F. Bader, "A precoding-based PAPR reduction technique for UF-OFDM and filtered-OFDM modulations in 5G systems," 23th European Wireless Conference, Dresden, Germany, pp. 285–290, 2017.
[18] M.I. Al-Rayif, H.E. Seleem, A.M. Ragheb, and S.A. Alshebeili, "PAPR reduction in UFMC for 5G cellular systems," Electronics, vol. 9, no. 9, pp. 1–15, 2020.
[19] N. Taşpınar, and Ş. Şimşir, "PAPR reduction based on partial transmit sequence technique in UFMC waveform," 14th Iberian Conf. Inf. Syst. Technol. (CISTI), Coimbra, Portugal, pp. 1-6, 2019.
[20] I. Baig, U. Farooq, N.U. Hasan, M. Zghaibeh, A. Sajid, and U.M. Rana, "A low PAPR DHT precoding based UFMC scheme for 5G communication systems," 6th International Conference on Control, Decision and Information Technologies (CoDIT), Paris, France, pp. 425–428, 2019.
[21] S.A. Fathy, M.N.A. Ibrahim, S.S. Elagooz, and H.M. El-Hennawy, "Efficient SLM technique for PAPR reduction in UFMC systems," 36th National Radio Science Conference (NRSC 2019), Port Said, Egypt, pp. 118–125, 2019.
[22] K. Liu, Y. Ge, and Y. Liu, "An efficient piecewise nonlinear companding transform for PAPR reduction in UFMC systems," IEEE/CIC International Conference on Communications in China (ICCC), Changchun, China, pp. 730–734, 2019.
[23] T. Jiang, and Y. Wu, "An overview: peak-to-average power ratio reduction techniques for OFDM signals," IEEE Transactions on Broadcasting, vol. 54, no. 2, pp. 257–268, 2008.
[24] T.T. Nguyen, and L. Lampe, "On partial transmit sequences for PAR reduction in OFDM systems," IEEE Transactions on Wireless Communications, vol. 7, no. 2, pp. 746–755, 2008.
[25] M. Bidar, M. Mouhoub, and S. Sadaoui, "Discrete firefly algorithm: a new metaheuristic approach for solving constraint satisfaction problems," IEEE Congress on Evolutionary Computation (CEC), Rio de Janeiro, Brazil, pp. 1–8, 2018.

Received 4 April 2023